Journal of Molecular Structure 998 (2011) 69–78

Contents lists available at ScienceDirect

Journal of Molecular Structure

journal homepage: www.elsevier.com/locate/molstruc

# FT-IR, FT-Raman spectra and scaled quantum mechanical study of 4-amino-1-benzylpiperidine

S. Chandra [a], H. Saleem [b,*], Y. Erdogdu [c], S. Subashchandrabose [b], Akhil R. Krishnan [b], M.T. Gulluoglu [c]

[a] Department of Engg. Physics, Annamalai University, Annamalai Nagar 608 002, India
[b] Department of Physics, Annamalai University, Annamalai Nagar 608 002, India
[c] Department of Physics, Ahi Evran University, Kirsehir 40040, Turkey

ARTICLE INFO

*Article history:*
Received 19 February 2011
Received in revised form 6 May 2011
Accepted 9 May 2011
Available online 13 May 2011

*Keywords:*
FT-IR
FT-Raman
4A1BP
NBO
HOMO–LUMO

ABSTRACT

In this work, we report a combined experimental and theoretical study on molecular structure, vibrational spectra of 4-amino-1-benzyl piperidine (4A1BP). The FT-IR and FT-Raman spectrum have been recorded in the region 4000–400 $cm^{-1}$ and 3500–50 $cm^{-1}$ respectively. The molecular geometry, harmonic vibrational frequencies and bonding features of 4A1BP have been calculated by using density functional theory methods with B3LYP and 6-31G(d,p) basis set. Using the same basis set NBO analysis was performed. The calculated HOMO and LUMO energies show that the charge transfers occur with in the molecule. The theoretical FT-IR and FT-Raman spectra for the title molecule have been constructed. Mulliken charges were also calculated using B3LYP/6-31, 6-311, 6-311++G(d,p) level method.



## 1. Introduction

Piperidines are an important group of heterocyclic compounds in the field of medicinal chemistry owing to the fact that these can frequently be recognized in the structure of numerous naturally occurring alkaloid and synthetic compounds with interesting biological and pharmacological properties. Piperidine derivatives were also reported to possess analgesic [1,2] anti-inflammatory [2] central nervous system [3–7] local anaesthetic [3–8] anticancer [9] and antimicrobial activity [10]. Piperidine nucleus is also found in drugs as raloxifene, minaxidil [11] and as a raw material for preparing epoxy resins, corrosion inhibitors and antioxidant [12]. The vibrational studies of piperidine on theoretical studies of Density functional calculations were also reported [13–20].

The literature survey reveals DFT calculations and experimental studies have not been reported for the title compound (4A1BP) so far. To fulfill the lacunae, the current investigation of FT-IR, FT-Raman and theoretical studies are carried out and reported in this study.

## 2. Experimental details

A pure chemical of 4A1BP was obtained from Sigma–Aldrich Company, USA and was used as such without further purification after checking its melting point 110 °C to record FT-Raman and FT-IR spectra. The FT-Raman spectrum of 4A1BP has been recorded using 1064 nm line of Nd-YAG laser source of 200 mw for excitation in the region 3500–50 $cm^{-1}$ on a BRUKER IFS 66V spectrophotometer. The FT-IR spectrum of this compound was recorded in the region 4000–400 $cm^{-1}$ on IFS66V spectrophotometer in KBr pellet. The spectrum was recorded at the room temperature with a scanning speed of 30 $cm^{-1}min^{-1}$ and the spectral width 2.0 $cm^{-1}$. The frequencies for all sharp bands are accurate to 4 $cm^{-1}$. The spectral measurements were carried out at RSIC, IIT, at Chennai.

## 3. Computational details

The DFT (B3LYP) calculations were performed using Gaussian 03W [21] program package without any constraint on the geometry [22]. Geometries of the model 4A1BP were first optimized with full relaxation on the potential energy surfaces ($C_2$—$N_{15}$—$C_{16}$—$C_{17}$ and $C_3$—$C_4$—$N_{30}$—$H_{31}$ dihedral angles) at B3LYP/6-31G(d,p) level and the resultant geometries were used as inputs for further calculations at DFT(B3LYP) level. The curves between dihedral angles ($C_2$—$N_{15}$—$C_{16}$—$C_{17}$ and $C_3$—$C_4$—$N_{30}$—$H_{31}$) and relative energy are shown in Fig. 1. Optimized structural parameters were used in the vibrational frequency calculations at DFT level to characterize all stationary points as minima using GAUSSVIEW molecular visualizing program [23] along with the assignments were made with a high degree of accuracy.

### 3.1. Prediction of Raman intensities

The Raman activities ($S_i$) calculated with Gaussian 03 program converted to relative Raman intensities ($I_i$) using the following

* Corresponding author. Tel.: +91 9443879295.
*E-mail address:* saleem_h2001@yahoo.com (H. Saleem).

0022-2860/$ - see front matter © 2011 Elsevier B.V. All rights reserved.
doi:10.1016/j.molstruc.2011.05.014

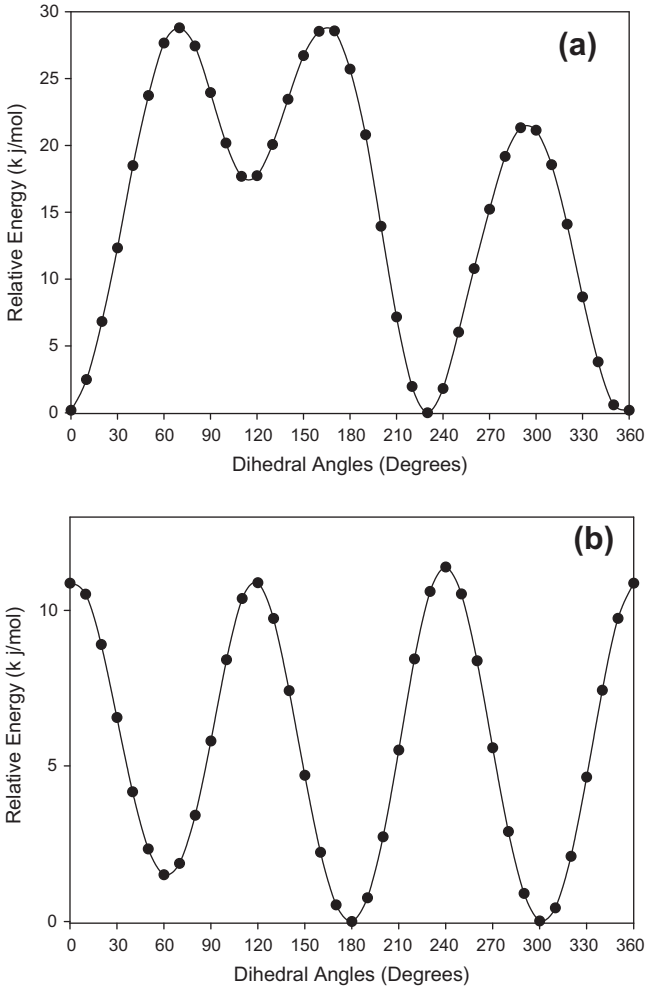


**Fig. 1.** Dihedral angles $\left(\frac{a \Rightarrow C2-N15-C16-C17}{b \Rightarrow C3-C4-N30-H31}\right)$ – relative energy curve of 4A1BP.

relationship derived from the intensity theory of Raman scattering [24,25]

$$I_i = \frac{f(v_o - v_i)^4 S_i}{v_i[1 - \exp(-hcv_i/kt)]} \quad (1)$$

where $v_0$ is the exciting frequency in $cm^{-1}$, $v_i$ the vibrational wavenumber of the $i$th normal mode, $h$, $c$, and $k$ are the fundamental constants and $f$ is a suitably chosen common normalization factor for all peak intensities.

## 4. Results and discussion

### 4.1. Molecular geometry

The optimized geometric parameters calculated by B3LYP with 6-31G(d,p) as the basis set is listed in Table 1. To the best of our knowledge, experimental data on the geometric structure of 4A1BP is not available in the literature. However, Vayner et al. [19] presented some bond distances, bond angles and dihedral angles for piperidine molecule. Erdogdu and Gulluoglu [12] observed that the C—N—C bond angles are slightly shorter than C—C bond distances. It is seen that the similar trend has been observed in our present study also. The molecular structure of 4A1BP is shown in Fig. 2.

### 4.2. Vibrational assignments

The spectral assignments have been performed on the recorded FT-IR (solid phase) and FT-Raman spectra based on the theoretically predicted wavenumbers by density functional B3LYP/6-31G(d,p) method have been collected in Table 2. The FT-IR and FT-Raman spectrum of 4A1BP is shown in Figs. 3 and 4. None of the predicted vibrational frequencies have any imaginary frequency, implying that the optimized geometry is located at the local minimum point on the potential energy surface. We know that DFT potentials systematically overestimate the vibrational wavenumbers. These discrepancies are corrected either by computing anharmonic corrections explicitly or by introducing a scaled field [26] or directly scaling the calculated wavenumbers with the proper factor [27]. The scaling factor of 0.9668 is used for B3LYP method. After scaling with a scaling factor, the deviation from the experiments is less than 10 $cm^{-1}$ with few exceptions. All 90 fundamental vibrations are active in both IR and Raman. Comparison of the frequencies calculated at DFT method using 6-31G(d,p) basis set with experimental values reveals that the B3LYP method show very good agreement with experimental observation due to inclusion of electron correlation for this method.

#### 4.2.1. $NH_2$ vibrations

The molecule under consideration posses $NH_2$ group and hence six internal modes of vibration are possible such as: (i) symmetric stretching ($v_s$), (ii) asymmetric stretching ($v_{as}$), (iii) scissoring ($\delta$), (iv) rocking ($\rho$), (v) wagging ($\omega$) and the torsional mode ($\tau$). The $NH_2$ group has two (N—H) stretching vibrations; one being asymmetric and other symmetric. The frequency of asymmetric vibration is higher than that of symmetric one. If the two NH bonds of the $NH_2$ group are symmetric, these modes satisfy an empirical relation is suggested by Bellamy and Williams [28] as $v_{sy} = 345.5 + 0.876 v_{asy}$, where $v_{sy}$ and $v_{asy}$ are wave numbers.

According to Socrates [29] the frequencies of amino group appear around 3500–3300 $cm^{-1}$ for $NH_2$ stretching. The harmonic asymmetric and symmetric stretching modes of $NH_2$ group are computed at 3418 (mode no: 90) and 3337 (mode no: 89) $cm^{-1}$, respectively. The observed bands at 3366 $cm^{-1}$ (FT-IR) and 3307 $cm^{-1}$ (FT-Raman) are ascribed to asymmetric and symmetric $NH_2$ stretching respectively. Bellamy and Williams [30] and Mancy et al. [31] suggested that the $NH_2$ scissoring mode lie in the region 1590–1650 $cm^{-1}$. In accordance with their conclusion, the $NH_2$ scissoring mode is identified with a weak band at 1601 and 1602 $cm^{-1}$ in FT-IR and FT-Raman respectively.

The computed —$NH_2$ scissoring vibration at 1598 $cm^{-1}$ (B3LYP: 72) is in agreement with the recorded spectral data. Similar trend has been followed in the case of 2-amino-5-methyl pyridine [32]. The observed bands 1170: FT-IR/1174: FT-Raman 1020 $cm^{-1}$ and 971 $cm^{-1}$ in FT-IR are attributed to the twisting mode of the $NH_2$ group. The theoretically scaled $NH_2$ twisting vibrations at 1170, 1021 and 971 (B3LYP-mode nos: 49, 39, 35) exactly correlates with experimental observations.

The theoretically calculated $\rho NH_2$ modes 207, 246 $cm^{-1}$ (B3LYP; 6, 7) have been found to be consistent with the recorded Raman spectral (211, 248 $cm^{-1}$) values. The wagging mode of the $NH_2$ group appears in the range 600–800 $cm^{-1}$ [33]. In this study, the weak bands observed at 786, 867 $cm^{-1}$ in FT-IR (787 $cm^{-1}$: FT-Raman) are assigned to $\omega NH_2$ mode. The theoretically computed values 796, 862 $cm^{-1}$ (B3LYP: 25, 28) shows good agreement with experimental values.

#### 4.2.2. $CH_2$ vibrations

For the assignment of $CH_2$ group frequencies, basically six fundamentals can be associated to each $CH_2$ group, namely: (i) $CH_2$ symmetric stretching, (ii) $CH_2$ asymmetric stretching, (iii) $CH_2$

**Table 1**
Geometrical parameters of 4A1BP (bond length, bond angle and dihedral angle).

| Parameters Bond lengths (Å) | B3LYP | Exp.[a] | Parameters Bond angle (°) | B3LYP | Exp.[a] | Dihedral angle (°) | B3LYP | Exp[a]. |
|---|---|---|---|---|---|---|---|---|
| $C_1$—$C_5$ | 1.532 | 1.523 | $C_4$—$C_5$—$H_{12}$ | 108.4 | 109.2 | $H_7$—$C_1$—$C_5$—$C_4$ | −48.72 | |
| $C_1$—$H_7$ | 1.107 | 0.980 | $C_4$—$C_5$—$H_{13}$ | 110.3 | 109.2 | $H_{14}$—$C_2$—$N_{15}$—$C_1$ | −63.52 | |
| $C_1$—$H_8$ | 1.096 | | $H_{12}$—$C_5$—$H_{13}$ | 107.6 | 109.4 | $H_{14}$—$C_2$—$N_{15}$—$C_{16}$ | 68.73 | |
| $C_1$—$N_{15}$ | 1.462 | 1.460 | $C_1$—$N_{15}$—$C_2$ | 112.2 | 111.0 | $C_2$—$C_3$—$C_4$—$C_5$ | 54.42 | |
| $C_2$—$C_3$ | 1.532 | 1.520 | $C_1$—$N_{15}$—$C_{16}$ | 114.2 | | $C_2$—$C_3$—$C_4$—$H_{11}$ | −61.85 | |
| $C_2$—$H_6$ | 1.096 | 0.980 | $C_2$—$N_{15}$—$C_{16}$ | 114.2 | | $C_2$—$C_3$—$C_4$—$N_{30}$ | 175.0 | |
| $C_2$—$H_{14}$ | 1.107 | 0.980 | $N_{15}$—$C_{16}$—$C_{17}$ | 117.0 | | $H_9$—$C_3$—$C_4$—$C_5$ | −66.41 | |
| $C_2$—$N_{15}$ | 1.462 | 1.461 | $N_{15}$—$C_{16}$—$H_{28}$ | 107.1 | | $H_9$—$C_3$—$C_4$—$H_{11}$ | 177.3 | |
| $C_3$—$C_4$ | 1.532 | 1.518 | $N_{15}$—$C_{16}$—$H_{29}$ | 107.1 | | $H_9$—$C_3$—$C_4$—$N_{30}$ | 54.18 | |
| $C_3$—$H_9$ | 1.095 | 0.980 | $C_{17}$—$C_{16}$—$H_{28}$ | 109.0 | | $H_{10}$—$C_3$—$C_4$—$C_5$ | 175.9 | |
| $C_3$—$H_{10}$ | 1.098 | 0.980 | $C_{17}$—$C_{16}$—$H_{29}$ | 109.0 | | $H_{10}$—$C_3$—$C_4$—$H_{11}$ | 59.65 | |
| $C_4$—$C_5$ | 1.532 | 1.523 | $H_{28}$—$C_{16}$—$H_{29}$ | 106.9 | | $H_{10}$—$C_3$—$C_4$—$N_{30}$ | −63.46 | |
| $C_4$—$H_{11}$ | 1.107 | 0.980 | $C_{16}$—$C_{17}$—$C_{18}$ | 120.9 | | $C_3$—$C_4$—$C_5$—$C_1$ | −54.42 | |
| $C_4$—$N_{30}$ | 1.467 | | $C_{16}$—$C_{17}$—$C_{19}$ | 120.9 | | $C_3$—$C_4$—$C_5$—$H_{12}$ | 66.41 | |
| $C_5$—$H_{12}$ | 1.095 | 0.980 | $C_{18}$—$C_{17}$—$C_{19}$ | 118.1 | | $C_3$—$C_4$—$C_5$—$H_{13}$ | −175.9 | |
| $C_5$—$H_{13}$ | 1.098 | 0.980 | $C_{17}$—$C_{18}$—$C_{20}$ | 121.0 | | $H_{11}$—$C_4$—$C_5$—$C_1$ | 61.85 | |
| $N_{15}$—$C_{16}$ | 1.467 | | $C_{17}$—$C_{18}$—$H_{21}$ | 119.3 | | $H_{11}$—$C_4$—$C_5$—$H_{12}$ | −177.3 | |
| $C_{16}$—$C_{17}$ | 1.524 | | $C_{20}$—$C_{18}$—$H_{21}$ | 119.5 | | $H_{11}$—$C_4$—$C_5$—$H_{13}$ | −59.65 | |
| $C_{16}$—$H_{28}$ | 1.096 | | $C_{17}$—$C_{19}$—$C_{22}$ | 121.0 | | $N_{30}$—$C_4$—$C_5$—$C_1$ | −175.0 | |
| $C_{16}$—$H_{29}$ | 1.096 | | $C_{17}$—$C_{19}$—$H_{23}$ | 119.3 | | $N_{30}$—$C_4$—$C_5$—$H_{12}$ | −54.18 | |
| $C_{17}$—$C_{18}$ | 1.402 | | $C_{22}$—$C_{19}$—$H_{23}$ | 119.5 | | $N_{30}$—$C_4$—$C_5$—$H_{13}$ | 63.46 | |
| $C_{17}$—$C_{19}$ | 1.402 | | $C_{18}$—$C_{20}$—$C_{24}$ | 120.0 | | $C_3$—$C_4$—$N_{30}$—$H_{31}$ | 62.01 | |
| $C_{18}$—$C_{20}$ | 1.395 | | $C_{18}$—$C_{20}$—$H_{25}$ | 119.8 | | $C_3$—$C_4$—$N_{30}$—$H_{32}$ | 177.9 | |
| $C_{18}$—$H_{21}$ | 1.087 | | $C_{24}$—$C_{20}$—$H_{25}$ | 120.0 | | $C_5$—$C_4$—$N_{30}$—$H_{31}$ | −177.9 | |
| $C_{19}$—$C_{22}$ | 1.395 | | $C_{19}$—$C_{22}$—$C_{24}$ | 120.0 | | $C_5$—$C_4$—$N_{30}$—$H_{32}$ | −62.00 | |
| $C_{19}$—$H_{23}$ | 1.087 | | $C_{19}$—$C_{22}$—$H_{26}$ | 119.8 | | $H_{11}$—$C_4$—$N_{30}$—$H_{31}$ | −57.93 | |
| $C_{20}$—$C_{24}$ | 1.395 | | $C_{24}$—$C_{22}$—$H_{26}$ | 120.0 | | $H_{11}$—$C_4$—$N_{30}$—$H_{32}$ | 57.96 | |
| $C_{20}$—$H_{25}$ | 1.086 | | $C_{20}$—$C_{24}$—$C_{22}$ | 119.5 | | $C_1$—$N_{15}$—$C_{16}$—$C_{17}$ | 65.65 | |
| $C_{22}$—$C_{24}$ | 1.395 | | $C_{20}$—$C_{24}$—$H_{27}$ | 120.2 | | $C_1$—$N_{15}$—$C_{16}$—$H_{28}$ | −171.6 | |
| $C_{22}$—$H_{26}$ | 1.086 | | $C_{22}$—$C_{24}$—$H_{27}$ | 120.2 | | $C_1$—$N_{15}$—$C_{16}$—$H_{29}$ | −57.10 | |
| $C_{24}$—$H_{27}$ | 1.086 | | $C_4$—$N_{30}$—$H_{31}$ | 109.6 | | $C_2$—$N_{15}$—$C_{16}$—$C_{17}$ | −65.64 | |
| $N_{30}$—$H_{31}$ | 1.018 | | $C_4$—$N_{30}$—$H_{32}$ | 109.6 | | $C_2$—$N_{15}$—$C_{16}$—$H_{28}$ | 57.10 | |
| $N_{30}$—$H_{32}$ | 1.018 | | $H_{31}$—$N_{30}$—$H_{32}$ | 105.9 | | $C_2$—$N_{15}$—$C_{16}$—$H_{29}$ | 171.6 | |
| Bond angles (°) | | | Dihedrals (°) | | | $N_{15}$—$C_{16}$—$C_{17}$—$C_{18}$ | 89.38 | |
| $C_5$—$C_1$—$H_7$ | 109.3 | 109.3 | $H_7$—$C_1$—$C_5$——$C_4$ | −67.38 | | $N_{15}$—$C_{16}$—$C_{17}$—$C_{19}$ | −89.41 | |
| $C_5$—$C_1$—$H_8$ | 109.7 | | $H_7$—$C_1$—$C_5$—$H_{12}$ | 172.5 | | $H_{28}$—$C_{16}$—$C_{17}$—$C_{18}$ | −32.33 | |
| $C_5$—$C_1$—$N_{15}$ | 110.5 | 109.3 | $H_7$—$C_1$—$C_5$—$H_{13}$ | 54.66 | | $H_{28}$—$C_{16}$—$C_{17}$—$C_{19}$ | 148.8 | |
| $H_7$—$C_1$—$H_8$ | 106.7 | | $H_8$—$C_1$—$C_5$—$C_4$ | 175.8 | | $H_{29}$—$C_{16}$—$C_{17}$—$C_{18}$ | −148.8 | |
| $H_7$—$C_1$—$N_{15}$ | 112.2 | 109.3 | $H_8$—$C_1$—$C_5$—$H_{12}$ | 55.82 | | $H_{29}$—$C_{16}$—$C_{17}$—$C_{19}$ | 32.32 | |
| $H_8$—$C_1$—$N_{15}$ | 108.1 | | $H_8$—$C_1$—$C_5$—$H_{13}$ | −62.07 | | $C_{16}$—$C_{17}$—$C_{18}$—$C_{20}$ | −178.1 | |
| $C_3$—$C_2$—$H_6$ | 109.7 | 109.3 | $N_{15}$—$C_1$—$C_5$—$C_4$ | 56.66 | | $C_{16}$—$C_{17}$—$C_{18}$—$H_{21}$ | 2.44 | |
| $C_3$—$C_2$—$H_{14}$ | 109.3 | 109.3 | $N_{15}$—$C_1$—$C_5$—$H_{12}$ | −63.38 | | $C_{19}$—$C_{17}$—$C_{18}$—$C_{20}$ | 0.63 | |
| $C_3$—$C_2$—$N_{15}$ | 110.5 | 109.8 | $N_{15}$—$C_1$—$C_5$—$H_{13}$ | 178.7 | | $C_{19}$—$C_{17}$—$C_{18}$—$H_{21}$ | −178.7 | |
| $H_6$—$C_2$—$H_{14}$ | 106.7 | 109.3 | $C_5$—$C_1$—$N_{15}$—$C_2$ | −58.84 | | $C_{16}$—$C_{17}$—$C_{19}$—$C_{22}$ | 178.1 | |
| $H_6$—$C_2$—$N_{15}$ | 108.1 | 109.3 | $C_5$—$C_1$—$N_{15}$—$C_{16}$ | 168.8 | | $C_{16}$—$C_{17}$—$C_{19}$—$H_{23}$ | −2.44 | |
| $H_{14}$—$C_2$—$N_{15}$ | 112.2 | 109.3 | $H_7$—$C_1$—$N_{15}$—$C_2$ | 63.52 | | $C_{18}$—$C_{17}$—$C_{19}$—$C_{22}$ | −0.63 | |
| $C_2$—$C_3$—$C_4$ | 111.1 | 110.7 | $H_7$—$C_1$—$N_{15}$—$C_{16}$ | −68.73 | | $C_{18}$—$C_{17}$—$C_{19}$—$H_{23}$ | 178.7 | |
| $C_2$—$C_3$—$H_9$ | 109.8 | 109.3 | $H_8$—$C_1$—$N_{15}$—$C_2$ | −179.0 | | $C_{17}$—$C_{18}$—$C_{20}$—$C_{24}$ | −0.17 | |
| $C_2$—$C_3$—$H_{10}$ | 109.4 | 109.3 | $H_8$—$C_1$—$N_{15}$—$C_{16}$ | 48.72 | | $C_{17}$—$C_{18}$—$C_{20}$—$H_{25}$ | −179.7 | |
| $C_4$—$C_3$—$H_9$ | 108.4 | 109.1 | $H_6$—$C_2$—$C_3$—$C_4$ | −175.8 | | $H_{21}$—$C_{18}$—$C_{20}$—$C_{24}$ | 179.1 | |
| $C_4$—$C_3$—$H_{10}$ | 110.3 | 109.8 | $H_6$—$C_2$—$C_3$—$H_9$ | −55.82 | | $H_{21}$—$C_{18}$—$C_{20}$—$H_{25}$ | −0.40 | |
| $H_9$—$C_3$—$H_{10}$ | 107.6 | 109.4 | $H_6$—$C_2$—$C_3$—$H_{10}$ | 62.07 | | $C_{17}$—$C_{19}$—$C_{22}$—$C_{24}$ | 0.17 | |
| $C_3$—$C_4$—$C_5$ | 109.0 | 110.3 | $H_{14}$—$C_2$—$C_3$—$C_4$ | 67.38 | | $C_{17}$—$C_{19}$—$C_{22}$—$H_{26}$ | 179.7 | |
| $C_3$—$C_4$—$H_{11}$ | 107.5 | 109.2 | $H_{14}$—$C_2$—$C_3$—$H_9$ | −172.5 | | $H_{23}$—$C_{19}$—$C_{22}$—$C_{24}$ | −179.1 | |
| $C_3$—$C_4$—$N_{30}$ | 109.9 | | $H_{14}$—$C_2$—$C_3$—$H_{10}$ | −54.66 | | $H_{23}$—$C_{19}$—$C_{22}$—$H_{26}$ | 0.40 | |
| $C_5$—$C_4$—$H_{11}$ | 107.5 | 109.2 | $N_{15}$—$C_2$—$C_3$—$C_4$ | −56.66 | | $C_{18}$—$C_{20}$—$C_{24}$—$C_{22}$ | −0.30 | |
| $C_5$—$C_4$—$N_{30}$ | 109.9 | | $N_{15}$—$C_2$—$C_3$—$H_9$ | 63.38 | | $C_{18}$—$C_{20}$—$C_{24}$—$H_{27}$ | −179.7 | |
| $H_{11}$—$C_4$—$N_{30}$ | 112.7 | | $N_{15}$—$C_2$—$C_3$—$H_{10}$ | −178.7 | | $H_{25}$—$C_{20}$—$C_{24}$—$C_{22}$ | 179.2 | |
| $C_1$—$C_5$—$C_4$ | 111.1 | 110.2 | $C_3$—$C_2$—$N_{15}$—$C_1$ | 58.84 | | $H_{25}$—$C_{20}$—$C_{24}$—$H_{27}$ | −0.18 | |
| $C_1$—$C_5$—$H_{12}$ | 109.0 | 109.2 | $C_3$—$C_2$—$N_{15}$—$C_{16}$ | −168.8 | | $C_{19}$—$C_{22}$—$C_{24}$—$C_{20}$ | 0.30 | |
| $C_1$—$C_5$—$H_{13}$ | 109.4 | 109.2 | $H_6$—$C_2$—$N_{15}$—$C_1$ | 179.0 | | $C_{19}$—$C_{22}$—$C_{24}$—$H_{27}$ | 179.7 | |

[a] Ref. [50].

scissoring and (iv) $CH_2$ rocking which belongs to in-plane ($A'$) species vibrations. In addition to that: (i) $CH_2$ wagging of $CH_2$ group would be expected to be depolarized for out-of-plane ($A''$) symmetry species.

The C—H stretching vibrations of the methylene group are at lower frequencies than those of the aromatic C—H ring stretching. A major coincidence of theoretical values (DFT-vibrations: 81 and 76) with that of experimental evaluation is found in the asymmetric (2922 $cm^{-1}$/Raman) and symmetric (2849 $cm^{-1}$/FT-IR) stretching vibrations of methylene (—$CH_2$) moiety. Similar trend has been observed by Tasal et al. [34] in the case of 3-(piperidin-1-yl-methyl)-1, 3-benzoxazol-2(3H)-one. The antisymmetric $CH_2$ stretching vibrations are generally observed in the region 2900–3000 $cm^{-1}$, while the symmetric stretch will appear between 2850 and 2900 $cm^{-1}$ [35].

In the present assignment, the $CH_2$ bending modes follow in decreasing wave number, the general order is: $CH_2$ deformation > $CH_2$ wagging > $CH_2$ twisting > $CH_2$ rocking. Since

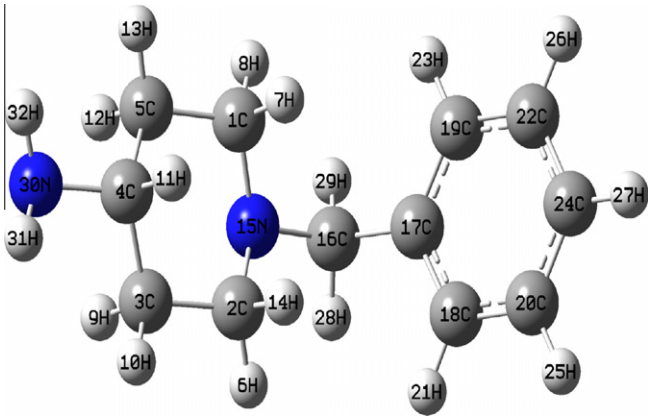


**Fig. 2.** Optimized molecular structure of 4A1BP.

the bending modes involving hydrogen atom attached to the central carbon fall into the 1450–875 $cm^{-1}$ range. There is extensive vibrational coupling of these modes with $CH_2$ deformation particularly with the $CH_2$ twist. It is notable that both $CH_2$ scissoring and $CH_2$ rocking were sensitive to the molecular conformation. The fundamental $CH_2$ vibrations are able to show scissoring, wagging, twisting and rocking modes and presently appear in the expected frequency regions 1500–800 $cm^{-1}$ [18].

These vibrations revealed to be mixed with C—C and C—N stretching. In FT-IR spectrum of 4A1BP, the weak bands at 1466 $cm^{-1}$ and 1453 $cm^{-1}$ assigned to $CH_2$ scissoring vibration. The same vibration in FT-Raman is observed at 1453 $cm^{-1}$. The theoretical wave number of $CH_2$ scissoring vibrations 1452 and 1466 $cm^{-1}$ (B3LYP-mode nos: 67, 68) are incidentally coincide very well with experimental values. These assignments find support from the work of Gulluoglu et al. [11] and are within the frequency intervals given by Vedal et al. [18].

The FT-IR wagging mode in the range 1296–1366 $cm^{-1}$ corresponding to $CH_2$ was calculated to be in the range 1296–1371 $cm^{-1}$ (B3LYP-mode nos: 54, 61). The present assignments agree well with the values available in literature [11]. In the present work, the FT-IR frequencies observed in the range 971–1170 $cm^{-1}$ have been assigned to $CH_2$ twisting vibrations. The corresponding vibrations appear in the FT-Raman spectrum at 1174 $cm^{-1}$. The theoretically computed values in the range 971–1170 $cm^{-1}$ (mode nos: 35, 42, 44, 45, 49) shows excellent agreement with experimental data by B3LYP/6-31G(d,p) method. These assignments find support from the work of Sebastian and Sundaraganesan [20] in the case of 4-hydroxy piperidine.

The $CH_2$ rocking vibrations calculated to be 487, 396 $cm^{-1}$ (B3LYP-mode nos: 17, 12) is also in excellent agreement with recorded value of 487 $cm^{-1}$ (FT-IR/Raman) and 395 $cm^{-1}$ in Raman spectrum. This is in agreement with Gulluoglu et al. [11].

*4.2.3. C—H vibrations*

The heteroaromatic structure shows the presence of C—H stretching with in the region 3000–3100 $cm^{-1}$ which is the characteristic region for the ready identification of C—H stretching vibrations and typically exhibit weak bands compared with the aliphatic C—H stretching [36–38]. The most organic compounds containing C—H bands show $SP^3$ C—H stretching in the region 2850–3000 $cm^{-1}$, whereas $SP^2$ C—H stretching appears above 3000 $cm^{-1}$ [34]. The vibrations (B3LYP-mode nos: 84–88) assigned to aromatic C—H stretching in the region 3045–3079 $cm^{-1}$, which are in agreement with experimental assignment in the range of 3003–3061 $cm^{-1}$. These results are supported by the literature [34]. The aromatic CH in-plane bending modes of benzene and its derivatives are observed in the region 1000–1300 $cm^{-1}$ [39]. The bands observed in the FT-IR spectrum 1296, 1170, 1143 $cm^{-1}$ and FT-Raman spectrum 1287, 1174 $cm^{-1}$ are assigned to C—H in-plane bending vibration of 4A1BP. The theoretically computed values by B3LYP method at 1296 and 1140 (mode nos: 54 and 46) show good agreement with recorded data. The C—H out-of-plane deformation is observed between 1000 and 700 $cm^{-1}$ [40]. Generally C—H out-of-plane deformation modes owned by highest wave numbers have weaker intensity than those absorbing at lower wave numbers [41]. Accordingly, in 4A1BP compound the C—H out-of-plane deformation are observed at 906, 867 and 829 $cm^{-1}$. The scaled frequencies (958, 934, 897, 829, 803 (B3LYP-mode nos: 33, 31, 30, 27, 26) reproduce well the experimental ones. These assignments also find support from Tasal et al. [34].

*4.2.4. C—C vibrations*

Tasal et al. [34] assigned C—C stretching vibrations are in the range 1453–1625 $cm^{-1}$ in the case of 3-(piperidine-1-yl-methyl)-1, 3-benzoxazol-2(3H)-one. As can be seen from Table 2, the observed frequencies in the range 1453–1602 $cm^{-1}$ are belongs to the same mode. While the harmonic frequencies are in the range of 1436–1595 $cm^{-1}$ (DFT mode nos: 65, 69–71). In the present work we observed C—C—C stretching at 1003 (Raman) and 983 $cm^{-1}$ (FT-IR) and ring trigonal bending at 971 $cm^{-1}$ (FT-IR). These assignments are supported by theoretical values 1015 and 977 $cm^{-1}$ (DFT mode nos: 38, 36) respectively. The bands (FT-IR) at 603, (620: Raman), 487, 464, (463: Raman), 416 $cm^{-1}$ are designated to $\beta$(C—C—C) and $\gamma$(C—C—C) vibrations respectively. The theoretically calculated C—C—C in-plane and out-of-plane bending modes have been found to be consistent with the recorded spectra values.

*4.2.5. C—$NH_2$, C—N and C—N—C vibrations*

The FT-Raman/FT-IR stretching mode 1088 $cm^{-1}$ corresponding to C—$NH_2$ moiety was calculated to be 1062 $cm^{-1}$ (DFT: mode no-40). The C—$NH_2$ out-of-plane vibration calculated at 251 $cm^{-1}$ (DFT: mode no-8) which is also in agreement with the assignment in the experimental data. The identification of C—N vibrations is a very difficult task, since the mixing of several bands is possible in the region. Silverstein et al. [42] assign C—N stretching absorption in the region 1382–1266 $cm^{-1}$ for aromatic amines. In 3-(piperidine-1-yl-methyl)-1,3-benzoxazol-2(3H)-one, the C—N stretching bands are found to be in the region 1024–1271 $cm^{-1}$ [34]. The C—N stretching mode is assigned in the region 1055–1224 $cm^{-1}$ for 2-methyl piperidine by Erdogdu and Gulluoglu [12]. In the present work, the FT-IR/FT-Raman bands observed at 1088 $cm^{-1}$ and 1131 $cm^{-1}$: FT-IR are assigned to C—N stretching mode. The theoretically calculated values of C—N stretching vibrations in the region 1062–1101 $cm^{-1}$ (mode nos: 40, 42 and 43) coincides with experimental data and also find support from literature values [20]. The C—N—C in-plane bending vibration assigned at 633 $cm^{-1}$ (FT-IR) and the C—N—C out-of-plane bending vibration found at 395 $cm^{-1}$ (Raman). These assignments are in agreement with calculated frequencies by B3LYP/6-31G(d,p) method (mode nos: 20 and 11) and also find supported from the literature values in the case of nicotinamide [43].

## 5. Thermodynamic properties

Entropy of the title compound is presented in Table 3. Scale factors have been recommended [44] for an accurate prediction in determining the zero-point vibration energies (ZPVE), and the entropy, $S_{vib}$ (T). The variations in the ZPVE's seem to be insignificant.

**Table 2**
Vibrational wave numbers obtained for 4A1BP at B3LYP/6-31G(d,p).

| Mode no. | Experimental ($cm^{-1}$) | | Theoretical (B3LYP/6-31G(d,p)) | | | | |
|---|---|---|---|---|---|---|---|
| | FT-IR | FT-Raman | Scaled freq.[a] | $I_{IR}$[b] | $I_{Raman}$[c] | TED[d] % | Vibrational assignments |
| 1 | | | 38 | 0.40 | 100 | $\Gamma_{CCCH}(33) + \Gamma_{CCCN}(23) + \Gamma_{CCNC}(19) + \Gamma_{HCNC}(21)$ | Ring torsion |
| 2 | | | 45 | 0.17 | 52.1 | $\Gamma_{CNCH}(24) + \Gamma_{CNCC}(21) + \Gamma_{CCCC}(10) + \Gamma_{CCN}(13)$ | Ring out of plane bending |
| 3 | | 101 ms | 72 | 0.28 | 30.8 | $\Gamma_{CCCN}(36) + \Gamma_{CCNC}(34)$ | Ring torsion |
| 4 | | | 109 | 0.48 | 7.22 | $\Gamma_{CCCC}(15) + \Gamma_{CCCN}(10)$ | $\gamma$C—$NH_2$ + Ring out of plane bending |
| 5 | | | 202 | 0.30 | 10.0 | $\Gamma_{CCCC}(22) + \Gamma_{CNCH}(13)$ | Ring out of plane bending |
| 6 | | | 207 | 2.41 | 0.05 | $\Gamma_{HNCC}(27) + \Gamma_{CNCH}(16) + \Gamma_{CNCC}(12) + \delta_{CNC}(10)$ | $\rho NH_2 + \rho CH_2$ in $R_1$ |
| 7 | | | 246 | 2.72 | 0.66 | $\Gamma_{HNCC}(53) + \Gamma_{HNCH}(11)$ | $\rho NH_2 + \rho CH_2$ in $R_1$ |
| 8 | | 211 | 251 | 1.81 | 2.83 | $\nu_{CC}(12) + \delta_{CCN}(10)$ | $\rho CH_2 + \gamma$C—$NH_2 + \gamma$C—H |
| 9 | | 248 vw | 255 | 21.7 | 4.01 | $\delta_{CCC}(31) + \delta_{CNC}(14)$ | $tNH_2$ |
| 10 | | | 327 | 4.93 | 0.33 | $\delta_{CCN}(26) + \Gamma_{HCCN}(25) + \Gamma_{CCCN}(15) + \Gamma_{HNCH}(12)$ | $tNH_2 + \rho CH_2$ |
| 11 | | | 345 | 9.02 | 0.97 | $\Gamma_{CCCH}(20) + \Gamma_{HCNC}(14) + \delta_{CNC}(12)$ | $\rho CH_2 + \gamma$C—N—C |
| 12 | | 395 vw | 396 | 0.24 | 0.11 | $\delta_{CCC}(22) + \Gamma_{HCNC}(18) + \delta_{CNC}(16)$ | $\rho CH_2$ in $R_2$ |
| 13 | | | 401 | 1.99 | 2.49 | $\delta_{CCC}(15) + \Gamma_{CCCC}(13) + \Gamma_{CNCH}(12)$ | $\gamma$C—C—C + $\rho CH_2$ |
| 14 | 416 vw | | 403 | 0.01 | 0.03 | $\Gamma_{CCCC}(64) + \Gamma_{CCCH}(37)$ | $\gamma$C—C—C in $R_2$ |
| 15 | 464 vw | 463 vw | 453 | 0.94 | 2.33 | $\Gamma_{CCCH}(17)$ | $\rho CH_2 + \gamma$C—C—C + $\omega NH_2$ in $R_1$ |
| 16 | | | 481 | 8.60 | 2.60 | $\delta_{CCC}(12) + \nu_{CC}(11)$ | $\gamma$C—C—C + $\gamma$C—H in $R_2$ + $\rho CH_2$ in $R_1$ |
| 17 | 487 w | 487 vw | 487 | 0.00 | 1.12 | $\delta_{CCN}(22) + \delta_{CCC}(11) + \delta_{CNC}(11)$ | $\rho CH_2$ + Ring deformation in $R_1$ |
| 18 | 603 vw | | 559 | 5.01 | 1.65 | $\delta_{CCC}(14)$ | Ring deformation |
| 19 | | 620 vw | 611 | 0.00 | 3.07 | $\delta_{CCC}(58) + \delta_{CCH}(20)$ | Ring deformation in $R_2$ |
| 20 | 633 vw | | 640 | 12.7 | 1.30 | $\delta_{CCN}(10)$ | $\rho CH_2 + \beta$C—N—C + $\gamma$C—H in $R_1$ |
| 21 | 700 s | | 690 | 23.4 | 1.29 | $\Gamma_{CCCH}(58) + \Gamma_{CCCC}(27)$ | $\gamma$C—H |
| 22 | | | 723 | 8.55 | 12.8 | $\nu_{CN}(33)$ | Ring breathing + $\rho CH_2 + \gamma$C—H |
| 23 | 740 vs | 742 w | 754 | 10.3 | 1.68 | $\nu_{CN}(25) + \nu_{CC}(15)$ | Ring breathing + $\gamma$C—H |
| 24 | | | 795 | 0.87 | 1.13 | $\nu_{CC}(27) + \delta_{HNC}(18) + \delta_{HNCC}(14)$ | $\rho CH_2$ |
| 25 | | | 796 | 10.3 | 1.74 | $\Gamma_{HCCN}(14) + \delta_{CC}(10)$ | $\omega NH_2 + tNH_2 + \gamma$C—H |
| 26 | 786 vw | 787 w | 803 | 36.8 | 3.51 | $\delta_{CCC}(29) + \delta_{CCN}(12)$ | $\omega NH_2 + \gamma$C—H + $\beta$CCC + ring breathing in $R_2$ |
| 27 | 829 vw | 824 w | 829 | 0.01 | 2.59 | $\Gamma_{HCCH}(100)$ | $\gamma$C—H |
| 28 | 867 vw | | 862 | 65.6 | 1.95 | $\Gamma_{HNCC}(19) + \delta_{HNC}(16) + \nu_{CC}(10)$ | $\omega NH_2 + \rho CH_2 + \gamma$C—H |
| 29 | | | 876 | 0.00 | 0.09 | $\delta_{CCC}(31)$ | $\gamma$C—H + $\rho CH_2 + tNH_2$ |
| 30 | 906 vw | | 897 | 2.43 | 0.20 | $\Gamma_{CCCH}(84)$ | $\gamma$C—H |
| 31 | | | 934 | 0.65 | 0.51 | $\delta_{CCH}(8) + \nu_{CC}(8)$ | $\gamma$C—H + $\rho CH_2 + tNH_2$ |
| 32 | | | 935 | 0.75 | 0.56 | $\Gamma_{CCCH}(83)$ | $\rho CH_2+ \gamma$C—H in $R_1$ |
| 33 | | | 958 | 2.74 | 0.26 | $\nu_{CN}(25) + \delta_{CCN}(11)$ | $\gamma$C—H |
| 34 | | | 960 | 4.36 | 0.43 | $\Gamma_{HCCH}(69) + \Gamma_{HCCC}(14)$ | $\gamma$C—H + $\omega NH_2$ |
| 35 | | | 971 | 0.01 | 0.04 | $\Gamma_{HCCH}(25) + \nu_{CC}(10)$ | $tNH_2 + \beta$C—H + $tCH_2$ in $R_2$ |
| 36 | 971 vw | | 977 | 0.43 | 9.52 | $\delta_{CCC}(38) + \nu_{CC}(38)$ | Ring trigonal bending |
| 37 | 983 w | | 987 | 0.57 | 1.64 | $\nu_{CC}(56) + \nu_{CN}(17)$ | $\nu$C—C + $\omega CH_2$ in $R_1$ |
| 38 | | 1003 vs | 1015 | 1.95 | 4.65 | $\delta_{CCC}(53) + \delta_{CCH}(27) + \delta_{CCC}(13)$ | $\nu$C—C—C + $\beta$C—H |
| 39 | 1020 vw | | 1021 | 0.00 | 1.39 | $\nu_{CC}(45) + \delta_{HNC}(25)$ | $tNH_2 + \omega CH_2$ |
| 40 | 1029 vw | 1029 w | 1062 | 50.9 | 9.58 | $\nu_{CH}(41) + \nu_{CN}(24)$ | $\nu$C—$NH_2 + \beta$C—H + $\nu$C—N |
| 41 | | | 1065 | 11.7 | 0.14 | $\nu_{CC}(36) + \delta_{CCH}(32)$ | $\beta$C—H + $\nu$C—C + $tCH_2$ |
| 42 | 1088 ms | 1088 vw | 1092 | 7.28 | 1.23 | $\nu\nu_{CN}(24)$ | $tCH_2 + \nu$ C—C + $\omega NH_2 + \beta$C—H |
| 43 | 1131 vw | | 1101 | 7.79 | 1.36 | $\nu_{CN}(32) + \nu_{CC}(12)$ | $tCH_2 + \nu$ C—N + t($NH_2$) |
| 44 | | | 1123 | 11.3 | 1.59 | $\nu_{CN}(29)$ | $tCH_2 + \beta$C—H |
| 45 | | | 1136 | 0.08 | 0.83 | $\delta_{HCN}(19) + \delta_{CCH}(11)$ | $tCH_2 + \beta$C—H + $tNH_2$ |
| 46 | 1143 vw | | 1140 | 0.01 | 1.53 | $\delta_{CCH}(75) + \delta_{CC}(17)$ | $\beta$C—H |
| 47 | | | 1161 | 0.09 | 2.59 | $\delta_{CCH}(75) + \nu_{CC}(18)$ | $\beta$C—H |
| 48 | | | 1166 | 4.89 | 5.49 | $\nu_{CC}(63) + \nu_{CCH}(12)$ | $\nu$C—C + $\omega CH_2 + \beta$C—H |
| 49 | 1170 vw | 1174 vw | 1170 | 1.07 | 0.10 | $\delta_{CCH}(16) + \delta_{HNC}(13) + \delta_{HCN}(10)$ | $tNH_2 + tCH_2 + \beta$C—H |
| 50 | | | 1235 | 1.32 | 1.52 | $\delta_{CCH}(44) + \Gamma_{HCCN}(8)$ | $tCH_2 + \beta$C—H |
| 51 | | | 1236 | 1.14 | 4.49 | $\delta_{HNC}(26) + \delta_{CCH}(18)$ | $tCH_2 + tNH_2 + \beta$C—H |
| 52 | | | 1270 | 1.40 | 7.97 | $\delta_{CCH}(19) + \delta_{HCCH}(15) + \delta_{HCN}(14)$ | $tCH_2 + \beta$C—H |
| 53 | | | 1279 | 15.3 | 0.06 | $\delta_{CCC}(36) + \nu_{CN}(12)$ | $tCH_2 + \beta$C—H |
| 54 | 1296 vw | 1287 vw | 1296 | 0.04 | 0.21 | $\delta_{CCH}(21)$ | $\omega CH_2 + \beta$C—H + $tNH_2$ |
| 55 | | | 1302 | 9.36 | 1.44 | $\nu_{CC}(24) + \delta_{CCH}(20)$ | $tCH_2 + \beta$C—H + $\omega CH_2$ |
| 56 | | | 1307 | 1.01 | 0.42 | $\delta_{HCN}(22) + \delta_{CCH}(18) + \Gamma_{HCCH}(12)$ | Ring deformation + $\beta$C—H |
| 57 | | | 1315 | 1.48 | 0.54 | $\delta_{CCH}(49)$ | $tCH_2 + \beta$C—H + $\omega CH_2$ |
| 58 | 1314 vw | | 1322 | 19.6 | 1.77 | $\delta_{HCN}(33) + \delta_{CCH}(26) + \Gamma_{CCCH}(16) + \Gamma_{HCNC}(10)$ | $\omega CH_2 + \beta$C—H |
| 59 | 1341 vw | | 1340 | 0.90 | 0.01 | $\delta_{HCN}(21)$ | $\omega CH_2 + \beta$C—H + $tCH_2$ |
| 60 | | | 1365 | 19.1 | 1.51 | $\Gamma_{HCCH}(24) + \Gamma_{CCCH}(13)$ | $\omega CH_2 + \beta$C—H |
| 61 | | | 1371 | 4.23 | 0.63 | $\delta_{CCH}(23) + \delta_{HCN}(17) + \Gamma_{CNCH}(10)$ | $\omega CH_2 + \beta$C—H |
| 62 | 1366 w | | 1374 | 1.83 | 0.50 | $\Gamma_{HNCH}(17) + \delta_{HNC}(16) + \delta_{CCH}(12) + \nu_{CC}(11)$ | $tNH_2 + \beta$C—H + $tCH_2$ |
| 63 | | | 1426 | 6.44 | 3.92 | $\delta_{HCH}(33) + \Gamma_{HCNC}(26) + \Gamma_{CCCH}(26)$ | $\delta CH_2$ |
| 64 | | | 1430 | 0.39 | 4.24 | $\delta_{HCH}(26) + \Gamma_{HCCH}(12)$ | $\delta CH_2$ |
| 65 | | | 1436 | 3.91 | 0.05 | $\delta_{CCH}(49) + \nu_{CC}(27)$ | $\nu$C—C + $\beta$C—H + $tCH_2$ |
| 66 | | | 1448 | 4.03 | 0.85 | $\delta_{HCH}(26) + \Gamma_{HCCH}(18)$ | $\delta CH_2$ |
| 67 | 1453 w | 1453 vw | 1452 | 1.05 | 1.26 | $\delta_{HCH}(30) + \Gamma_{HCCH}(14) + \Gamma_{CNCH}(13)$ | $\delta CH_2$ |
| 68 | 1466 v w | | 1466 | 9.74 | 0.87 | $\delta_{HCH}(26) + \Gamma_{HCCH}(16) + \Gamma_{CCCH}(13)$ | $\delta CH_2$ |
| 69 | 1496 w | | 1477 | 5.55 | 0.26 | $\delta_{CCH}(62) + \nu_{CC}(27)$ | $\nu$C—C + $\beta$C—H |
| 70 | | | 1576 | 0.65 | 1.61 | $\nu_{CC}(69)$ | $\nu$C—C + $\beta$C—H |
| 71 | | 1585 vw | 1595 | 1.45 | 5.74 | $\nu_{CC}(67) + \delta_{CCH}(16)$ | $\nu$C—C + $\beta$C—H |
| 72 | 1601 vw | 1602 vw | 1598 | 23.1 | 1.95 | $\delta_{NHH}(53) + \delta_{CHH}(33)$ | $\delta NH_2$ |
| 73 | 2758 w | 2759 vw | 2796 | 19.3 | 1.37 | $\nu_{CH}(99)$ | $\nu C_4$—$H_{11}$ + $\nu$C—H in $CH_2$ |

(*continued on next page*)

**Table 2** (*continued*)

| Mode no. | Experimental ($cm^{-1}$) | | Theoretical (B3LYP/6-31G(d,p)) | | | | |
|---|---|---|---|---|---|---|---|
| | FT-IR | FT-Raman | Scaled freq.[a] | $I_{IR}$[b] | $I_{Raman}$[c] | TED[d] % | Vibrational assignments |
| 74 | 2801 ms | 2801 vw | 2810 | 13.5 | 0.20 | $\nu_{CH}(100)$ | $\nu$C—H in $CH_2$ + $\nu$C—H |
| 75 | | | 2818 | 100 | 5.43 | $\nu_{CH}(98)$ | $\nu$C—H in $CH_2$ + $\nu$C—H |
| 76 | | | 2912 | 31.1 | 3.65 | $\nu_{CH}(97)$ | $\nu_{sym}CH_2(C_{16}—H_{28}—H_{29})$ |
| 77 | | | 2914 | 34.0 | 2.81 | $\nu_{CH}(96)$ | $\nu_{sym}CH_2$ |
| 78 | | | 2916 | 29.1 | 5.41 | $\nu_{CH}(99)$ | $\nu_{sym}CH_2$ |
| 79 | 2932 vs | 2922 vw | 2937 | 43.0 | 0.82 | $\nu_{CH}(93)$ | $\nu$C—H |
| 80 | | | 2941 | 16.1 | 6.73 | $\nu_{CH}(93)$ | $\nu$CH |
| 81 | | | 2957 | 22.5 | 2.60 | $\nu_{CH}(98)$ | $\nu_{asym}(CH_2)$ |
| 82 | | | 2969 | 3.01 | 1.42 | $\nu_{CH}(97)$ | $\nu_{asym}(CH_2)$ in $R_1$ |
| 83 | | | 2973 | 42.1 | 3.49 | $\nu_{CH}(97)$ | $\nu_{asym}(CH_2)$ in $R_1$ |
| 84 | | 3003 | 3045 | 6.95 | 0.32 | $\nu_{CH}(100)$ | $\nu$(CH) in $R_2$ |
| 85 | 3027 w | | 3047 | 3.24 | 3.14 | $\nu_{CH}(100)$ | $\nu$(CH) in $R_2$ |
| 86 | | | 3059 | 5.32 | 4.21 | $\nu_{CH}(100)$ | $\nu$(CH) in $R_2$ |
| 87 | 3061 vw | 3055 | 3066 | 30.6 | 1.69 | $\nu_{CH}(100)$ | $\nu$(CH) in $R_2$ |
| 88 | | | 3079 | 17.1 | 10.95 | $\nu_{CH}(94)$ | $\nu$(CH) in $R_2$ |
| 89 | | 3307 vw | 3337 | 4.02 | 4.79 | $\nu_{CN}(100)$ | $\nu_{sym}(NH_2)$ |
| 90 | 3366 vw | | 3418 | 0.51 | 2.27 | $\nu_{NH}(100)$ | $\nu_{asym}(NH_2)$ |

$\nu$: Stretching, $\beta$: in-plane, $\gamma$: out-of-plane bending, $\omega$: wagging, t: twisting, $\delta$: scissoring, $\rho$: rocking, $\tau$: torsion.
s: strong, m: medium, w: weak, v: very.
[a] Scaling factor: 0.9668 for B3LYP/6-31g(d,p).
[b] Relative absorption intensities normalized with highest peak absorption equal to 100.
[c] Relative raman intensities normalized to 100.
[d] Total energy distribution calculated B3LYP/6-31g(d,p) level, TED less than 10% are not shown.

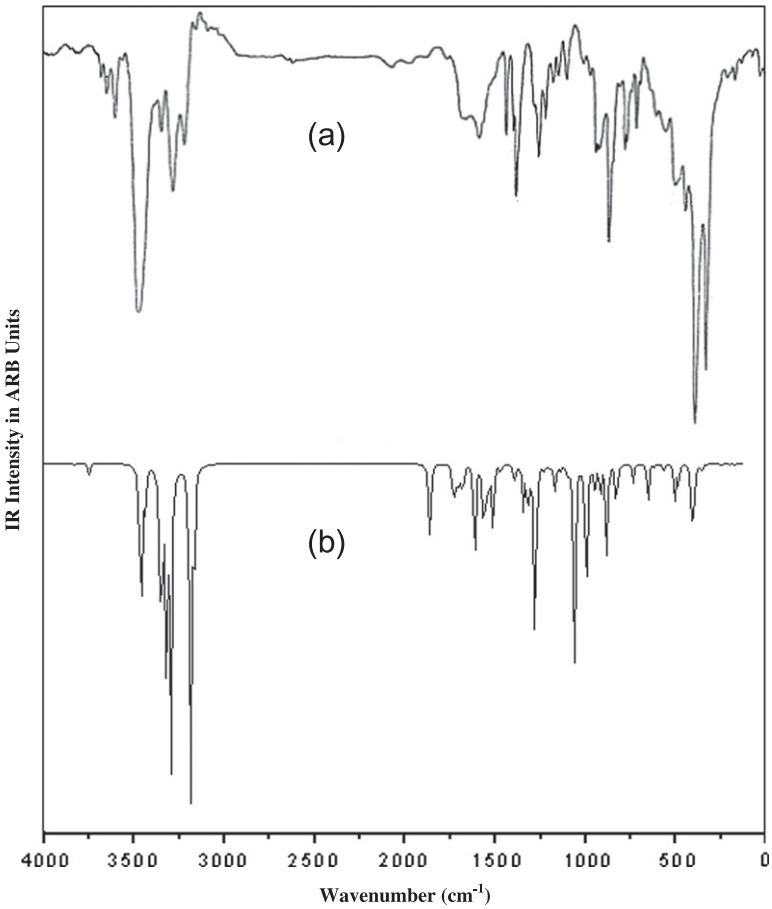


**Fig. 3.** Combined (a) experimental and (b) theoretical B3LYP/6-31G(d,p) IR spectrum of 4A1BP.

The total energies and the changes in the total entropy of 4A1BP at room temperature at different methods are also presented. Dipole moment is a measure of the asymmetry in the molecular charge distribution and is given as a vector in the three dimensions. The values dipole moments and energies for 4A1BP molecule were also calculated and listed. According to DFT (B3LYP) calculations, the

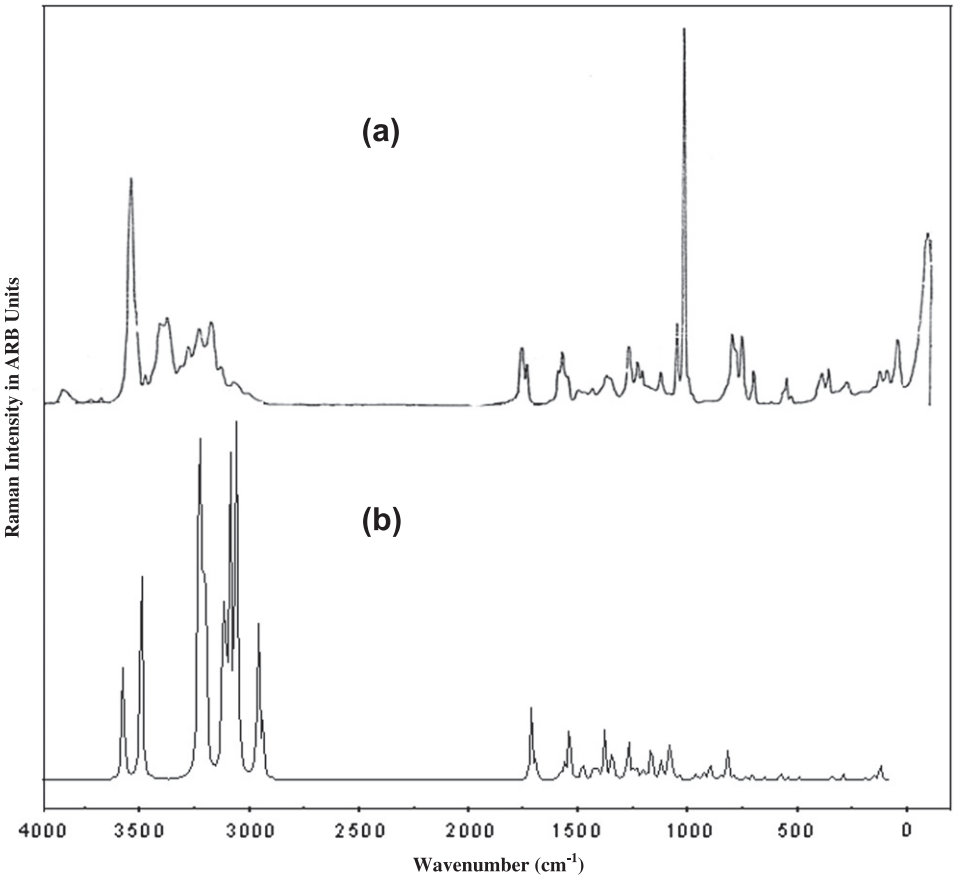


**Fig. 4.** Combined (a) experimental and (b) theoretical B3LYP/6-31G(d,p) Raman spectrum of 4A1BP.

**Table 3**
Theoretically computed energies, zero-point vibrational energies (kcal/mol), rotational constants (GHz), entropy (cal/mol $K^{-1}$), dipole moment (D) and energy gap (a.u) for 4A1BP.

| Parameters | B3LYP/6-31G(d,p) |
|---|---|
| Total energies | −577.636 |
| Zero point energy | 179.199 |
| Rotational constants | 1.5478, 0.3386, 0.3274 |
| *Entropy* | |
| Total | 111.812 |
| Translational | 41.634 |
| Rotational | 31.905 |
| Vibrational | 38.274 |
| Dipole moment (D) | 1.2029 |
| HOMO (a.u) | −0.20325 |
| LUMO (a.u) | −0.00067 |
| Energy gap | 0.20258 |

largest dipole moment and the lowest energy were observed for B3LYP/6-31G(d,p).

## 6. HOMO and LUMO analysis

Many organic molecules, containing conjugated π electrons are characterized by large values of molecular first hyperpolarizabilities, were analyzed by means of vibrational spectroscopy [45,46]. In most cases, even in the absence of inversion symmetry, the strongest bands in the Raman spectrum are weak in the IR spectrum and vice versa. But the intramolecular charge transfer from the donor to accepter group through a single–double bond conjugated path can induce large variations of both the molecular dipole moment and the molecular polarizability, making IR and Raman activity strong at the same time. The experimental spectroscopic behavior described above is well accounted for by *ab initio* calculations in π conjugated systems that predict exceptionally large Raman and infrared intensities for the some normal modes [45]. It is also observed in our title molecule the bands in FT-IR spectrum have their counterparts in Raman shows that the relative intensities in IR and Raman spectra are comparable resulting from the electron cloud movement through π conjugated frame work from electron donor to electron acceptor groups. The analysis of the wave function indicates that the electron absorption corresponds to the transition from the ground to the first excited state and is mainly described by one-electron excitation from the highest occupied molecular orbital (HOMO) to the lowest unoccupied molecular orbital (LUMO). The LUMO of π nature, (i.e. heterocyclic ring) is delocalized over the whole C—C and C—N bond. The HOMO–LUMO energy gap of 4A1BP was calculated at the B3LYP/6-31G(d,p) level and are shown in Fig. 5 which reveals that the energy gap reflect the chemical activity of the molecule. LUMO as an electron acceptor represents the ability to obtain an electron, HOMO represents the ability to donate an electron. The energy gap of 4A1BP was tabulated in Table 3.

## 7. NBO analysis

NBO analysis provides the most accurate possible 'natural Lewis structure' picture of ø, because all orbital details are mathematically chosen to include the highest possible percentage of the electron density. A useful aspect of the NBO method is that it gives information about interactions in both filled and virtual orbital spaces that could enhance the analysis of intra- and intermolecular

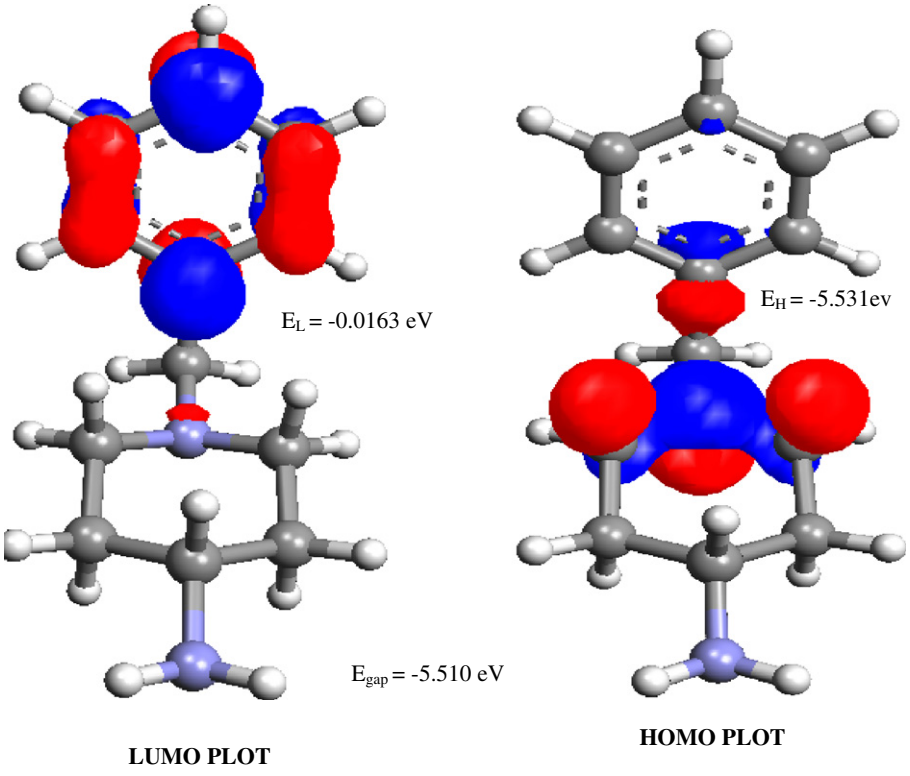


**Fig. 5.** Atomic orbital composition of the frontier molecular orbital for 4A1BP.

**Table 4**
Second order perturbation theory analysis of fock matrix in NBO basis for 4A1BP.

| Donor ($i$) | Occupancy | Acceptor($j$) | Occupancy | $E^{(2)}$ [a] (kJ mol$^{-1}$) | $E(j)-E(i)$ [b] (a.u) | $F(i,j)$ [c] (a.u) |
|---|---|---|---|---|---|---|
| $C_{17}$—$C_{19}$(1) | 1.97 | $C_{16}$—$C_{17}$ | 0.04 | 1.58 | 1.10 | 0.037 |
| | | $C_{17}$—$C_{18}$ | 0.02 | 3.27 | 1.27 | 0.057 |
| | | $C_{18}$—$H_{21}$ | 0.02 | 2.64 | 1.13 | 0.049 |
| | | $C_{19}$—$C_{22}$ | 0.02 | 3.12 | 1.27 | 0.056 |
| | | $C_{22}$—$H_{26}$ | 0.01 | 2.16 | 1.13 | 0.044 |
| $C_{17}$—$C_{19}$(2) | 1.65 | $N_{15}$—$C_{16}$ | 0.03 | 4.60 | 0.61 | 0.052 |
| | | $C_{18}$—$C_{20}$(2) | 0.33 | 20.1 | 0.28 | 0.067 |
| | | $C_{22}$—$C_{24}$(2) | 0.34 | 21.2 | 0.28 | 0.069 |
| $C_{18}$—$C_{20}$(1) | 1.98 | $C_{16}$—$C_{17}$ | 0.04 | 3.58 | 1.11 | 0.056 |
| | | $C_{17}$—$C_{18}$ | 0.02 | 3.36 | 1.27 | 0.058 |
| | | $C_{20}$—$C_{24}$ | 0.02 | 2.70 | 1.27 | 0.052 |
| | | $C_{24}$—$H_{27}$ | 0.01 | 2.37 | 1.14 | 0.047 |
| $C_{18}$—$C_{20}$(2) | 1.67 | $C_{17}$—$C_{19}$(2) | 0.35 | 20.7 | 0.29 | 0.069 |
| | | $C_{22}$—$C_{24}$(2) | 0.34 | 20.1 | 0.28 | 0.067 |
| $C_{22}$—$C_{24}$(1) | 1.98 | $C_{19}$—$C_{22}$ | 0.02 | 2.75 | 1.27 | 0.053 |
| | | $C_{19}$—$H_{23}$ | 0.02 | 2.50 | 1.13 | 0.048 |
| | | $C_{20}$—$C_{24}$ | 0.02 | 2.64 | 1.27 | 0.052 |
| | | $C_{20}$—$H_{25}$ | 0.01 | 2.42 | 1.14 | 0.047 |
| $C_{22}$—$C_{24}$(2) | 1.66 | $C_{17}$—$C_{19}$(2) | 0.35 | 19.8 | 0.29 | 0.067 |
| | | $C_{18}$—$C_{20}$(2) | 0.33 | 20.4 | 0.28 | 0.068 |

[a] $E^{(2)}$ means energy of hyper conjugative interaction (stabilization energy).
[b] Energy difference between donor and acceptor $i$ and $j$ NBO orbitals.
[c] $F(i,j)$ is the fork matrix element between $i$ and $j$ NBO orbitals.

interactions. The second order Fock matrix was carried out to evaluate the donor–acceptor interactions in the NBO analysis [47]. The interactions result is a loss of occupancy from the localized NBO of the idealized Lewis structure into an empty non-Lewis orbital. For each donor ($i$) and acceptor ($j$), the stabilization energy $E^{(2)}$ associated with the delocalization $i \rightarrow j$ is estimated as

$$E^{(2)} = \Delta E_{ij} = q_i \frac{F(i,j)^2}{\varepsilon_j - \varepsilon_i} \quad (2)$$

where $q_i$ is the donor orbital occupancy, are $\varepsilon_i$ and $\varepsilon_j$ diagonal elements and $F(i,j)$ is the off diagonal NBO Fock matrix element. Natural bond orbital analysis provides an efficient method for

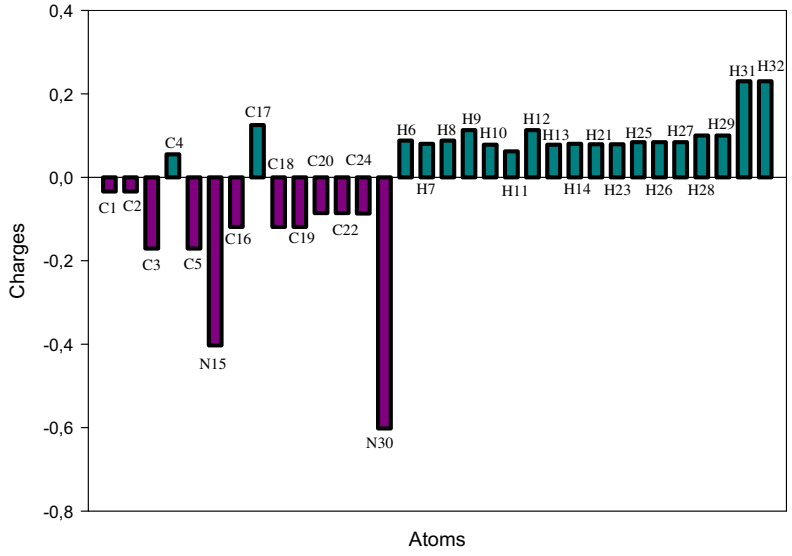


**Fig. 6.** Mulliken's plot for 4A1BP.

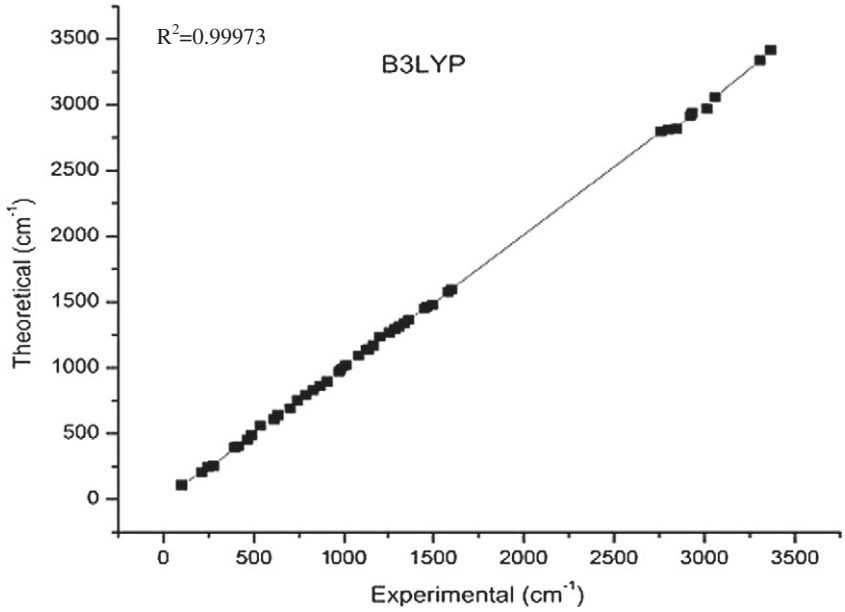


**Fig. 7.** Correlation coefficient between the experimental and theoretical frequencies of 4A1BP.

studying intra and intermolecular bonding and interaction among bonds, and also provides a convenient basis for investigating charge transfer or conjugative interaction in molecular systems. Some electron donor orbital, acceptor orbital and the interacting stabilization energy resulted from the second-order micro-disturbance theory are reported [48,49].

The larger the $E^{(2)}$ value, the more intensive is the interaction between electron donors and electron acceptors, i.e. the more donating tendency from electron donors to electron acceptors and the greater the extent of conjugation of the whole system. Delocalization of electron density between occupied Lewis-type (bond or lone pair) NBO orbitals and formally unoccupied (antibond or Rydgberg) non-Lewis NBO orbitals correspond to a stabilizing donor–acceptor interaction. NBO analysis has been performed on the molecule at the DFT/B3LYP/6-31G(d,p) level in order to elucidate the intramolecular, rehybridization and delocalization of electron density within the molecule are shown in Table 4. The NBO results suggest that the maximum energy (21.22 kJ mol$^{-1}$) transfers in $\pi$–$\pi^*$ transition.

## 8. Mulliken charges

The calculations of effective atomic charges plays an important role in the application of quantum mechanical calculations to molecular systems, because of atomic charge changes effect of dipole moment, molecular polarizability, electronic structure, acidity–basicity behavior and more a lot of properties of molecular systems. Our interest is in the comparison of different methods to describe the electron distribution in 4A1BP as broadly as possible, and assess the sensitivity of the calculated charges to changes in: (i) the choice of the basis set (ii) the choice of the quantum mechanical method. Mullikan charges are calculated by

determining the electron population of each atom as defined by basis sets. The result can, however, better be represented in graphical form as has been given in Fig. 6. From these results, it will be possible to say to the change to charge distribution by a change in basis set.

## 9. Conclusion

Vibrational spectral analysis is carried out using FT-IR (solid phase) and Raman spectroscopy for the 4A1BP. Assignments of the vibrational spectra have been facilitated by DFT calculation. A good correlation was found between the computed and experimental wavenumbers. The correlation coefficient between calculated and measured vibrational frequencies is 0.9997. The best fittings between calculated and measured vibrational frequencies were achieved by B3LYP theoretical level which is shown in Fig. 7. At this level, the deviation between calculated and experimental values is quite small for a given type of vibration. Therefore, this study confirms that the theoretical calculation of vibrational frequencies for 4A1BP is quite useful for the vibrational assignments and for predicting new vibrational frequencies. The theoretically constructed FT-IR and FT-Raman spectrum exactly coincides with experimentally observed FT-IR and FT-Raman spectrum respectively. Mulliken charges 4A1BP at different levels were calculated and the results discussed. HOMO, LUMO energies and HOMO–LUMO energy gap is also calculated. NBO results suggest that the maximum energy ($21.22\ kJ\ mol^{-1}$) transfers in $\pi$–$\pi^*$ transition.

## References

[1] G.J. Richardo, B.C. Juan, R.A. Mario, M. Roldan, C.R. Peinado, Fernando Spen. 47 (1979) 168.
[2] B.R. Jerom, K.H. Spencer, Eur. Pat. Appl. Ep 277794 (1998).
[3] R.V. Perumal, M. Adiraj, P. Shanmugapandian, Indian Drugs 38 (2001) 156.
[4] C.F. Bochringer, G.M.B.H. Shochne, Brit. Pat. Appl. BP 866488 (1961).
[5] C.R. Ganellin, R.G. Spickett, J. Med. Chem 8 (1965) 619.
[6] M. Nikolov, D. Stefanora, D. Chardanov, Acta Nerv. Super 16 (1974) 264.
[7] B. Kathleen, C. Jean-Peirre, H. Andre, Eur. Pat. Appl. Ep 169139 (1986).
[8] R.E. Hagenbach, H. Gysin, Experientia 8 (1952) 184.
[9] B. Heana, V. Dobre, I. Niculescu-Duvaz, J. Prakt. Chem 327 (1985) 667.
[10] I.G. Mobio, A.T. Soldatenkov, V.O. Fedrov, E.A. Ageev, N.D. Sergeeva, S. Lin, E.E. Stashenko, N.S. Prostakov, E.I. Andreeva, Khim. Farm. Zh. 23 (1989) 421.
[11] M.T. Gulluoglu, Y. Erdogdu, S. Yurdakul, J. Mol. Struct. 834 (2007) 540.
[12] Y. Erdogdu, M.T. Gulluoglu, Spectrochim. Acta A 74 (2009) 162.
[13] Yu.A. Pentin, O.S. Anisimova, Opt. Spectrosc. 26 (1968) 35.
[14] T. Hirokawa, T. Kimura, K. Ohno, H. Murata, Spectrochim. Acta A 36 (1980) 329.
[15] G. Marcotrigiano, L. Meanbue, G.C. Pellacani, J. Mol. Struct. 30 (1976) 85.
[16] Y. Okishi, Y. Imai, K. Aida, J. Inorg. Nucl. Chem. 13 (1973) 101.
[17] T.V. Titova, O.S. Anisimova, Opt. Spectrosc. 23 (1967) 495.
[18] D. Vedal, O. Ellestad, P. Klaboe, G. Hagen, Spectrochim Acta A 32 (1976) 877.
[19] E. Vayner, D.W. Ball, J. Mol. Struct. (THEOCHEM) 496 (2000) 175.
[20] S. Sebastian, N. Sundaraganesan, Spectrochim. Acta A 75 (2010) 941.
[21] Gaussian 03 Program, Gaussian Incl., Walling ford, CT, 2004.
[22] H.B. Schlegel, J. Comput. Chem. 3 (1982) 214.
[23] A. Frisch, A.B. Nielson, A.J. Holder, GAUSS VIEW User Manual, Gaussian Incl., Pittsburgh, PA, 2000.
[24] G. Keresztury, S. Holly, J. Varga, G. Besenyei, A.J. Wang, J.R. Durig, Spectrochim. Acta 49 A (1993) 2007.
[25] G. Keresztury, J.M. Chalmers and P.R. Griffith, Raman Spectroscopy: Theory in Hand Book of Vibrational spectroscopy, vol. 1. John wiley, New York.
[26] P. Pulay, G. Fogarasi, G. Ponger, J.E. Boggs, A. Vargha, Am. Chem. Soc. 105 (1983) 7073.
[27] A.P. Scott, L. Radom, J. Phys. Chem. 100 (1996) 16502.
[28] L.J. Bellamy, R.L. Williams, Spectrochim. Acta 9 (1957) 311.
[29] G. Socrates, Infrared, Raman Characteristic Group Frequencies Tables and Charts, third ed., Willey, Chichester, 2001.
[30] L.J. Bellamy, The Infrared Spectra of Complex Molecules, vol. 2, Chapman and Hall, London, 1980.
[31] S. Mancy, W.L. Peticoles, R.S. Toblas, Spectrochim. Acta A 35 (1979) 315.
[32] N. Sundaraganesan, C. Meganathan, M. Kurt, J. Mol. Struct. 891 (2008) 284.
[33] J.P. Abaraham, D. Sajan, I. Hubert Joe, V.S. Jayakumar, Spectrochim. Acta A 71 (2008) 355.
[34] E. Tasal, I. Sidir, Y. Gulselvan, C. Ogretir, T. Onkol, J. Mol. Struct. 923 (2009) 141.
[35] V. Krishnakumar, R.J. Xavier, T. Chidambarathanu, Spectrochim. Acta A 62 (2005) 931.
[36] A.A. El-Azhary, Spectrochim. Acta A 55 (1999) 2437.
[37] V. Krishnakumar, R. John Xavier, Indian J. Pure Appl. Phys. 41 (2003) 597.
[38] J. Coates, in: R.A. Meyers (Ed.), Interpretation of Infrared spectra, A Practical Approach, John Wiley and Sons Ltd., Chichester, 2000.
[39] M. Karabacak, M. Cinar, M. Kurt, J. Mol. Struct. 968 (2010) 108.
[40] N.P.G. Roeges, A Guide to the Complete Interpretation of Infrared Spectra of Organic Structures, Wiley, New York, 1994.
[41] K.R. Ambujakshan, V.S. Madhavan, H.T. Varghese, C.Y. Panicker, O.T. Arpaci, B.T. Gulbas, I. Yildiz, Spectrochim. Acta A 69 (2008) 782.
[42] M. Silverstein, G. Clayton Basseler, C. Moril, Spectrometric Identification of Organic Compounds, Wiley, New York, 1981.
[43] S. Ramalingam, S. Periyandi, M. Govindarajan, S. Mohan, Spectrochim. Acta A 75 (2010) 1552.
[44] M.A. Palafox, Int. J. Quant. Chem. 77 (2000) 661.
[45] N. Sundaraganesan, G. Elango, C. Meganathan, B. Karthikeiyan, M. Kurt, Mol. Simul. 35 (2009) 705.
[46] T. Vijayakumar, I.H. Joe, C.P.R. Nair, V.S. Jayakumar, Chem. Phys. 343 (2008) 83.
[47] M. Szafran, A. Komasa, E.B. Adamska, J. Mol. Struct. (THEOCHEM) 827 (2007) 101.
[48] C. James, A.A. Raj, R. Reghunathan, I.H. Joe, V.S. Jayakumar, J. Raman Spectrosc. 37 (2006) 1381.
[49] L. Jun-na, C. Zhi-rang, Y. Shen-fang, J. Zhejiang Univ. Sci 6B (2005) 584.
[50] A. Parkin, I.D.H. Oswald, S. Parsons, Acta Crystallogr. Sec. B 60 (2004) 219.